

Article

Study on the Stress Evolution and Strengthening Support Timing of the Retracement Channel under the Super-Thick Nappe

Ruojun Zhu ^{1,2}, Xizhan Yue ², Yudong Gao ^{3,*}, Xuesheng Liu ³, Xuebin Li ³ , Chengcheng Xie ³ and Kun Wang ^{3,4} ¹ College of Mining, China University of Mining and Technology, Xuzhou 221116, China; ahtzrj@163.com² China Coal Xinji Energy Co., Ltd., Huainan 232001, China; yuexixian1123@163.com³ College of Energy and Mining Engineering, Shandong University of Science and Technology, Qingdao 266590, China; liuxs@sdust.edu.cn (X.L.); xuebin9311@163.com (X.L.); chengxie3911@163.com (C.X.); wkun@sdust.edu.cn (K.W.)⁴ Engineering Research Center of Geothermal Resources Development Technology and Equipment, Ministry of Education, Jilin University, Changchun 130026, China

* Correspondence: gaoyudong1126@163.com

Abstract: The superposition effect of the advanced support pressure of the working face in the final mining stage and the lateral support stress of the roadway is a key factor affecting the stability of the retrace channel. To study the stress evolution of the retrace channel under the super-thick nappe and the timing of strengthening support, this paper takes the mining of the 360808 working face in Xinji No. 1 Mine as the engineering background, analyzes the occurrence conditions of the working face and the measured rock pressure law, and constructs a roof structure model of the retreat area. The UDEC discrete element numerical simulation software was used to analyze the evolution characteristics of concentrated stress and the failure law of surrounding rock around the retrace channel under gradual excavation conditions. Based on the relationship between the position of the main roof fracture and the stability of the surrounding rock of the retrace channel, the instability mechanism of the surrounding rock of the retrace channel was revealed. A mechanical model of the surrounding rock of the retrace channel under the condition of a gradient coal pillar was established, and the energy criterion K for the instability of the surrounding rock was obtained. The method of adding anchor cables to strengthen the support of the surrounding rock of the retrace channel was proposed. The results indicate that the accumulation of energy in the surrounding rock of the retrace channel is greater than the internal consumption of energy, which is the direct reason for the instability of the surrounding rock of the retrace channel. The time to strengthen the support of the roof is when the working face is 15 m away from the retrace channel. According to the analysis of on-site monitoring results, the roof convergence and the two-sides convergence before and after strengthening the support were reduced by 90 mm and 140 mm, respectively. Under the strengthening of support, the slope of the retrace channel in the 360808 working face is slight, without roof fall, and the surrounding rock of the channel is effectively controlled, which is of great significance for ensuring the safe application of the retrace channel. It has reference value for the safety production of surrounding mines and is conducive to promoting the sustainable development of local resource-based society and economy.

Keywords: super-thick nappe; retrace channel; strengthening support timing; numerical simulation; instability criterion



Citation: Zhu, R.; Yue, X.; Gao, Y.; Liu, X.; Li, X.; Xie, C.; Wang, K. Study on the Stress Evolution and Strengthening Support Timing of the Retracement Channel under the Super-Thick Nappe. *Sustainability* **2023**, *15*, 15677. <https://doi.org/10.3390/su152115677>

Academic Editor: Jianjun Ma

Received: 11 August 2023

Revised: 11 October 2023

Accepted: 2 November 2023

Published: 6 November 2023



Copyright: © 2023 by the authors. Licensee MDPI, Basel, Switzerland. This article is an open access article distributed under the terms and conditions of the Creative Commons Attribution (CC BY) license (<https://creativecommons.org/licenses/by/4.0/>).

1. Introduction

As the depth of coal mining gradually increases, the occurrence conditions of coal seams become more complex [1–4]. The roadway is influenced by the fractured zone of the coal rock structure, resulting in a high degree of stress concentration. When geological structures such as faults are close in spatial distance, the tectonic stresses overlap with each other, further increasing the stress of the coal rock mass [5–7]. Nappe is a complex

geological structure that has a significant impact on the stress distribution of tunnels. It refers to a thrust fault with a larger scale and a fault plane inclination angle below 30° [8–10]. At present, the rapid retracement of fully mechanized mining equipment mainly adopts the method of pre-excavating the retracement channel, and the structure of the nappe will lead to complex stress evolution process of the retracement channel, severe deformation and damage of the surrounding rock at the retracement channel edge, which is extremely unfavorable for the stability of the surrounding rock structure [11] and seriously restricts the safe and efficient production of the working face. In some areas, there is a problem of investing a large amount of support costs, but the support effect is still not ideal. Therefore, improving the coal mining rate and reducing mining costs are of great significance for the sustainable development of China's coal industry.

In recent years, scholars from China and other countries have conducted extensive research on the stress evolution of retracement channels under the influence of faults and the strengthening of support design, such as the use of FLAC^{3D} and boundary element numerical simulation methods. Li et al. [12–17] proposed the influence of different fault types on the stress of the retracement channel surrounding rock and the optimal support scheme for the retracement channel surrounding rock under the influence of corresponding faults. Taking the Barapukuria coal mine in Bangladesh as an example, Islam et al. [18] found that the deformation of rock layers near faults and the variation characteristics of the stress field in the surrounding rock of the retracement channel are under the influence of mining disturbances, emphasizing the occurrence of stress concentration at the location of fault fracture surfaces. Li et al. [19] established a coal pillar mechanical model based on the theory of falling arch, theoretically determined the width of the protective coal pillar between the retracement channel, and verified its mechanical response characteristics using the FLAC^{3D} calculation model. Qin et al. [20] proposed the relationship between the working resistance of hydraulic supports and the immediate roof sinking angle under the spatial relationship between the retracement channel and the roof fracture and determined the reasonable time for the arrangement of the retracement channel. Ma et al. [21] analyzed the failure process of tunnels under different conditions and discussed the failure process and final failure mode of tunnels. This study is of great significance for maintaining channel stability. Using a model test or a similar material test method, Zhang et al. [22,23] found in their research on the mechanism of roof cutting and pressure relief under the influence of faults that the vibration generated by roof fracture is relatively small, but the shear slip generated by faults releases a large amount of energy, causing severe vibration. Han et al. [24–27] combined the theory of elastic–plastic mechanics to analyze the stress evolution and instability failure process of surrounding rock under different conditions under the influence of faults. Ma et al. [28] reproduced the dynamic process and fracturing mode of the overlying rock layer through the M-JHB-4DLSM model experiment, which is of great significance for studying the impact effect of near-buried blasting tunnels. Through theoretical analysis and on-site measurement methods, Sainoki et al. [29,30] summarized the principle and applicability of stopping mining and yielding pressure during the final mining stage, combined with the pressure law of the working face. Wang et al. [31] proposed a mechanical model that considers the stress redistribution caused by mining in the working face and calculates the stress distribution on the fracture surface. Ma et al. [32] proposed a fully coupled thermo-elastoplastic damage constitutive model to study the mechanical response of specimens under dynamic loading, used to identify the damage situation of surrounding rock under dynamic loading conditions. Zhang et al. [33] obtained the relative displacement relationship between the roof and floor after a single support through monitoring and proposed the optimal and reasonable support timing. Dokht et al. [34–37] obtained the superposition effect of concentrated stress around the retracement channel and the mining support pressure of the working face, as well as the law of surrounding rock failure. Gu et al. [38] established a mechanical model for the remaining coal pillar, theoretically determined the critical stable width of the coal pillar, and conducted a sensitivity analysis on its geological and engineering factors to determine the position of stopping mining and yielding pressure. Zhu et al. [39] analyzed the influencing

factors of the main roof fracture position on the surrounding rock of the retracement channel and evaluated the difficulty of bracket retracement.

The above research results provide a theoretical basis and on-site practical experience for the stability control of surrounding rock in the retracement channel. However, based on the research status mentioned earlier, it can be concluded that Li et al.'s [12–17] research elucidated the structural deformation characteristics of tunnel surrounding rock under the influence of faults from the perspectives of mechanics and energy, but there is relatively little research on the impact of strong mining in the final mining stage on the gradual coal pillars. Wang et al. [31] proposed a mechanical structural model for roof sliding under the influence of faults and provided the timing for strengthening support through monitoring. The results have a certain degree of randomness. Dokht et al. [34–37] mainly studied the impact of strong mining during the final mining stage on the retracement channel. However, due to the particularity of thrust faults, there is insufficient research on the timing of strengthening support for retracement channels under this working condition.

Therefore, this article takes the mining of the 360808 working face under the structure of the thick nappe in Xinji No. 1 Mine as the engineering background. Firstly, UDEC discrete element numerical simulation software (UDEC 6.0 v6.0.336) is used to summarize the evolution law of deformation and failure of the surrounding rock of the retracement channel under the thick nappe structure. Then, based on the deformation situation of the surrounding rock of the retracement channel, an energy conversion criterion for the instability of the retracement channel surrounding rock is constructed, and a strengthened support design scheme for the retracement channel is proposed. Based on the deformation characteristic curve of the channel surrounding rock and combined with the on-site working conditions, the timing of strengthening support was determined, and the rationality of the design scheme was verified through on-site engineering. The research results are of great significance for guiding the safe and rapid retreat of the 360808 working face.

2. Project Overview

(1) Basic information about the working face.

The main structural form of the coal-bearing strata in Xinji No. 1 Mine is a monoclinic structure that leans toward the northeast or north. The coal seam outcrops are all located in the southern part of the minefield and developed in the in situ system of the Fufeng nappe structure. The dip angle of the middle and southern strata in the minefield is relatively gentle, generally 15° , and locally 35° . The dip angle in the north is relatively large, gradually increasing from 30° in the west to nearly 60° in the east, belonging to a typical thrust fault. There are weak interlayers and local fractured zones on the roof and floor of the main mining coal seam. There is a super-thick nappe structure with a thickness of 351–562 m above the 36 mining areas (as shown in Figure 1). The super-thick nappe structure is mainly composed of gneiss, and the lithology is mainly composed of granite gneiss and hornblende gneiss, presenting a mixed gray-black and gneissic structure.

Starting from the west of the 360808 working face, No. 3608 (6) mining area is transported up the mountain, 20 m east of the 8–9 exploration line, north neighbor 240805 working face goaf. The goaf of the 240818 working face is adjacent to the south. The northern upper part of the working face is the goaf of the 360806 working face (with a vertical distance of 63.2–91.5 m and an average of 77.4 m from this working face). The layout plan of the working face is shown in Figure 2. The main mining area of the 08 working face is the eighth coal seam, with an average coal thickness of 3.0 m. The coal mining method is a comprehensive mechanized coal mining method that moves toward the long wall and retreats. The roof is managed by the full height and full collapse method at once. The specific rock column diagram is shown in Figure 3.

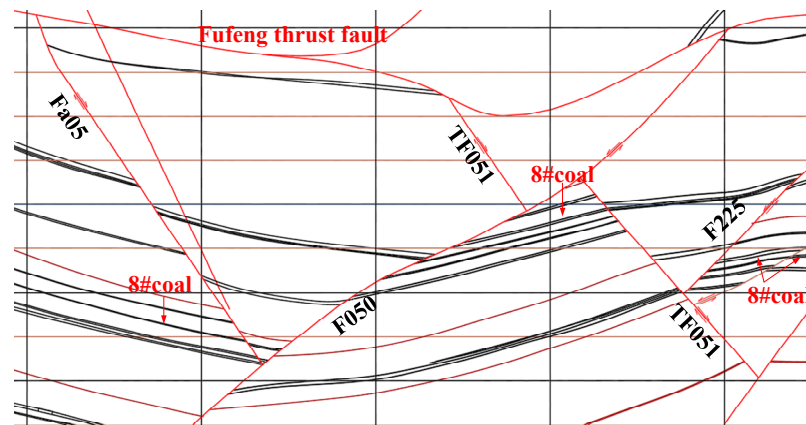


Figure 1. Nappe structure plane diagram.

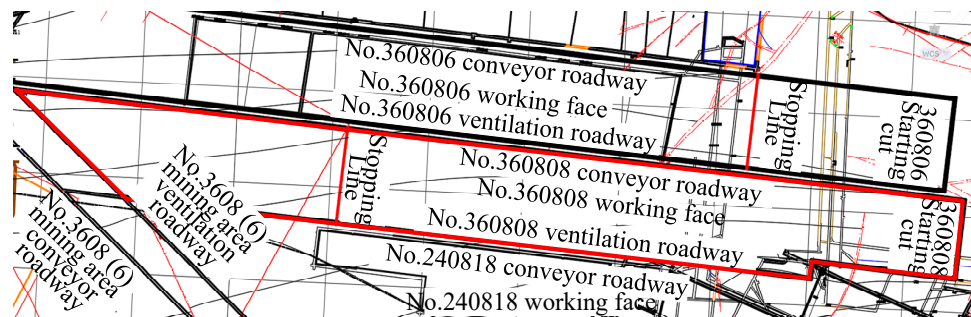


Figure 2. Layout plan of the No. 360808 working face (Selected area with thick red lines).

Rodman-shaped	Rock name	Average thickness/m	Rock description	Rock structure
	Gneiss	400	Directional distribution of dark and light minerals	Overburden
	Fine sandstone	11.72	Gray, fine-grained structure, stepped fracture	
	Sandy mudstone	8.16	Grey, sandy structure, massive structure	
	Silicarenite	34.88	Light gray, mainly quartz, calcareous cementation	
	Fine sandstone	3.86	Gray, fine-grained structure, stepped fracture	
	Mudstone	2.12	Gray, blocky, broken, jagged fracture	
	9# coal	1.14	Black, weak asphalt luster, blocky or scaly	
	Mudstone	4.13	Gray, blocky, broken, jagged fracture	Main roof
	Sandy mudstone	8.23	Grey, sandy structure, massive structure	
	Fine sandstone	4.07	Light gray, medium thick layer, siliceous cementation	Immediate roof
	Mudstone	0.89	Gray, blocky, broken, jagged fracture	
	8# coal	3.1	Black, weak glass luster, scaly structure	Coal
	Mudstone	8.35	Gray, blocky, broken, jagged fracture	Immediate floor
	Sandy mudstone	10.11	Grey, sandy structure, massive structure	Main floor

Figure 3. Rock stratum histogram.

(2) Design of the original support for the retracement channel.

To alleviate the tension of mining succession and improve the extraction rate of the working face, it is planned to pre-excavate the retracement channel near the stop mining line at the end of the working face. According to the “Mining Operation Regulations for 360808 Fully Mechanized Mining Face”, the original support method for the retracement channel was anchor rods, cables, and individual hydraulic props. The spacing between

individual hydraulic props is 1.1 m, and the support strength is 1600 kN/m. The anchor rod is a GM500 threaded steel anchor rod with a diameter of $\varphi = 22$ mm, length of 2.5 m, spacing of 800 mm \times 800 mm, and an average anchoring force of 100 kN. The anchor cable used is selected as 1 \times 19 S, $\Phi = 21.8$ mm prestressed steel strand production, with a length of 7.2 m and a spacing of 1200 \times 1200 mm, 5 in each row, with a bearing capacity of 583 kN, DW-25 (DW-31.5) single hydraulic prop with articulated beam, spacing of 1.1 m, and support strength of 1 MPa. The original support status of the retracement channel is shown in Figure 4.

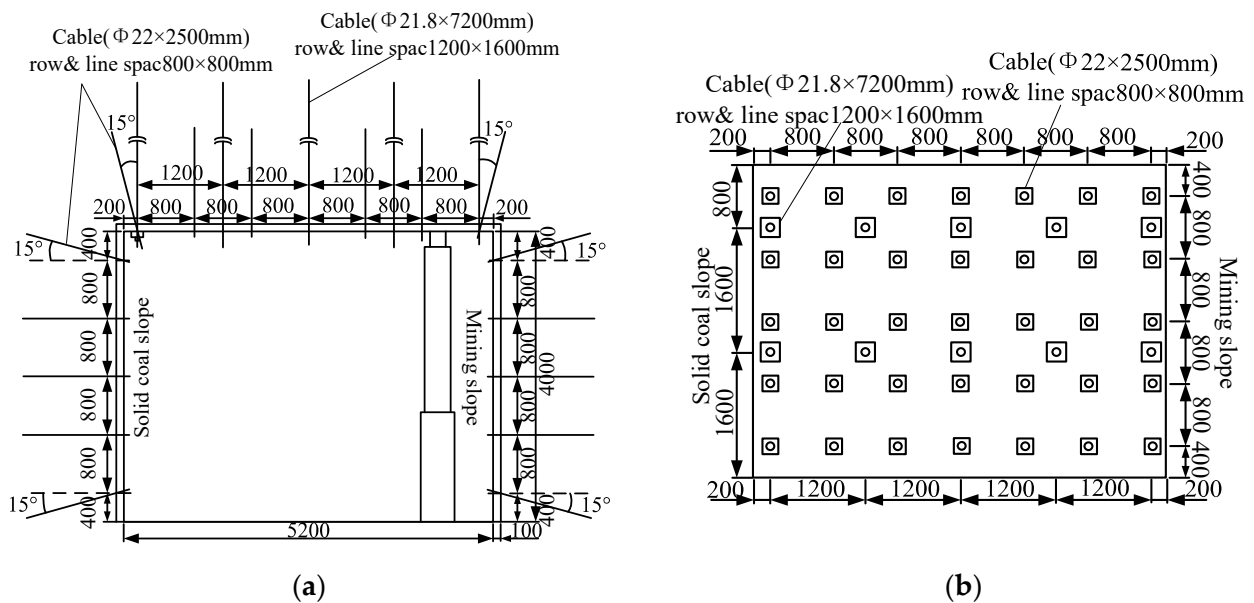


Figure 4. Schematic diagram of the original support status of the retracement channel. (a) Cross-section of retracement channel direction. (b) Top view.

3. Evolution Law of Deformation and Failure of Surrounding Rock in the Retracement Channel

3.1. Numerical Model Establishment and Simulation Plan

To understand the deformation and failure evolution of the surrounding rock of the retracement channel in the final mining stage of a fully mechanized mining face under the influence of the super-thick nappe, the discrete element numerical simulation software UDEC is considered for the numerical calculation to study the stress evolution and surrounding rock deformation process of the retracement channel in the final mining stage of the working face. Establish a numerical simulation basic model based on the actual engineering geological conditions on site, with a thickness of 400 m for the nappe, a mining height of 3 m, a mining length of 1000 m, the closest distance from the stop mining line to the horizontal projection of the fault of 500 m, and a size of 100 m for the right boundary protection coal pillar. The model size is length \times height = 1800 m \times 500 m.

The boundary condition of the model is to apply a horizontal constraint in the X-axis direction on the right boundary of the model and a vertical constraint in the Y-axis direction on the bottom of the model. Apply a vertical load to the top of the model to simulate the weight of the overburden and use the self-weight stress generated by the actual burial depth as the top-end face load. Apply the upper self-weight stress in the horizontal direction multiplied by the lateral pressure coefficient λ to simulate the initial crustal stress by loading. The mechanical model of the simulated coal rock mass adopts the Mohr–Coulomb model, and the joint mechanical model adopts the Coulomb slip model. The specific numerical model is shown in Figure 5, and the overall rock mechanics parameters of the model are shown in Table 1.

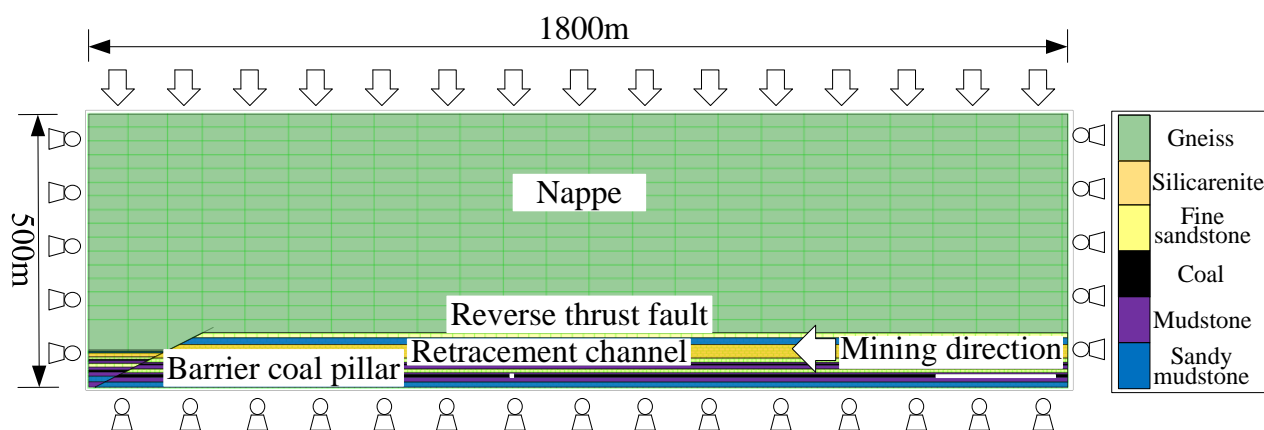


Figure 5. UDEC numerical calculation model.

Table 1. Physical and mechanical parameters of numerical model rock.

Serial Number	Rock Name	Thickness/m	Density kg/m ³	Tensile Strength/MPa	Elastic Modulus/GPa	Cohesion/MPa	The Angle of Internal Friction/°	Poisson Ratio
1	Gneiss	400	2763	11.2	44.8	15	40	0.25
2	Fine sandstone	12	2532	5.38	37.15	3.2	42	0.27
3	Sandy mudstone	8	2562	2.6	12.08	2.45	40	0.25
4	Silicarenite	35	2423	4.9	21.75	21	75	0.29
5	Fine sandstone	4	2532	5.38	37.15	3.2	42	0.27
6	Mudstone	2	2582	2.0	10.37	1.2	32	0.28
7	No. 9 coal seam	1	1401	0.3	2.79	0.8	29	0.32
8	Mudstone	4	2582	2.0	10.37	1.2	32	0.28
9	Sandy mudstone	8	2562	2.6	12.08	2.45	40	0.25
10	Fine sandstone	4	2532	5.38	37.15	3.2	42	0.27
11	Mudstone	1	2582	2.0	10.37	1.2	32	0.28
12	No. 8 coal seam	3	1378	0.4	1.32	0.8	29	0.31
13	Mudstone	8	2582	2.0	10.37	1.2	32	0.28
14	Sandy mudstone	10	2562	2.6	12.08	2.45	40	0.25

During the simulation process, corresponding displacement and stress monitoring points are selected for the roof convergence of the retracement channel and the two-sides convergence to monitor the roof convergence, the two-sides convergence, the maximum concentrated stress, and its position changes and to clarify the evolution law of deformation and failure of the surrounding rock of the retracement channel in the final mining stage. The specific simulation scheme is shown in Table 2 below.

Table 2. Simulation scheme design table.

Simulation Scheme	One	Two	Three	Four	Five	Six	Seven	Eight
Excavation length/m	800	100	60	10	10	10	5	5
Interval length from retreat channel/m	200	100	40	30	20	10	5	0

3.2. Stress Distribution and Evolution of Surrounding Rock in the Retracement Channel

The distribution and evolution of stress in the surrounding rock of the retracement channel under different simulation schemes are shown in Figure 6.

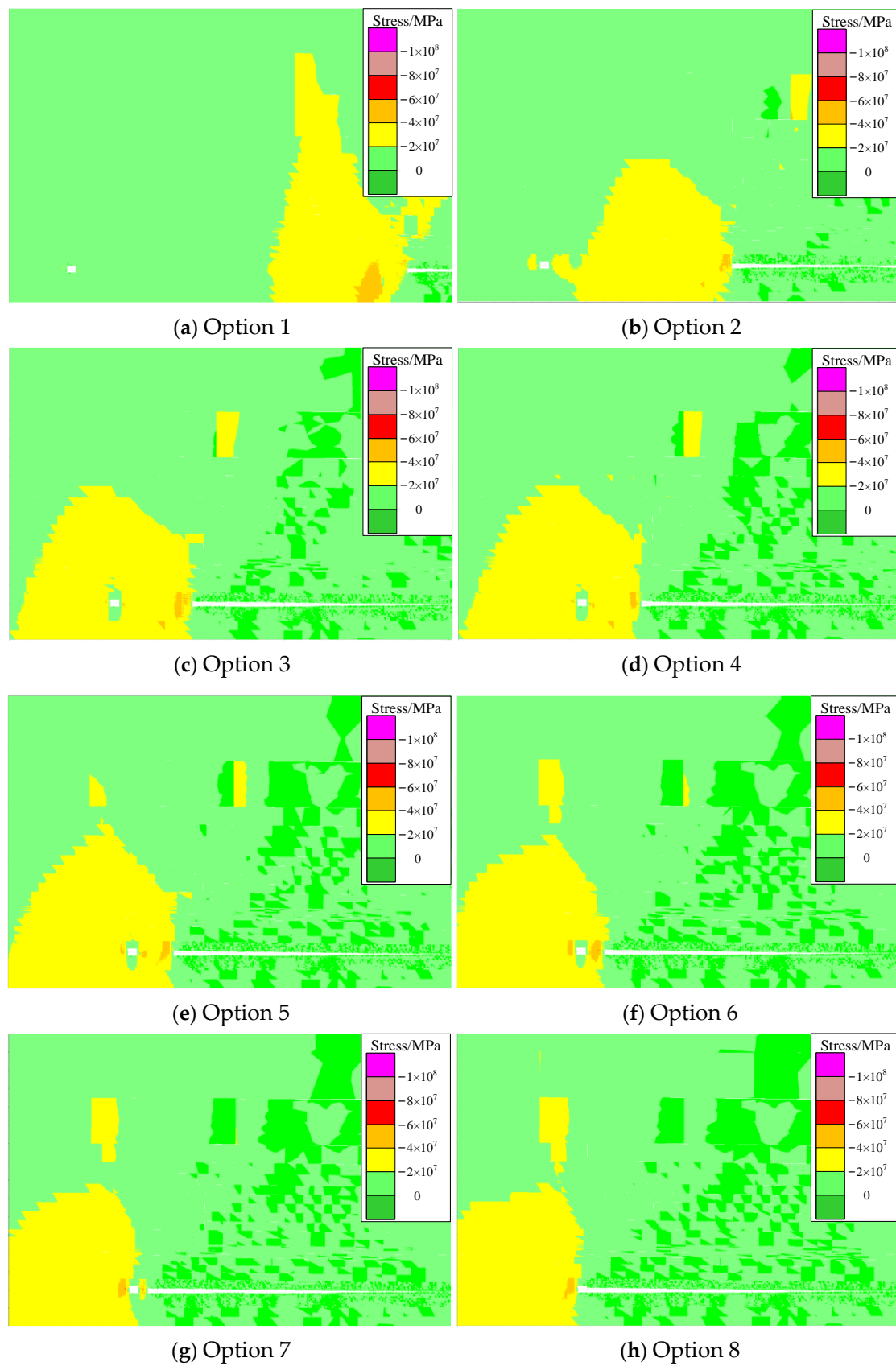


Figure 6. Stress cloud diagram at different distances from the working face to the retracement channel.

Based on the comprehensive analysis of the above stress cloud map, it can be concluded that when the working face is 200 m away from the retracement channel, it is not affected by mining outside the area affected by the advanced support pressure. When the working face is 100 m away from the retracement channel, the vertical stress in some areas of the retracement channel increases due to the influence of advanced support pressure. Afterward, as the working face continued to advance, the stress concentration areas on both sides of the retracement channel gradually increased, and the stress value increased.

Figure 7a shows the vertical stress distribution at different positions of the solid coal wall in the retracement channel during the mining process. From the figure, it can be seen that as the working face is mined, the stress on the outer side of the solid coal in the channel continues to increase. At 1 m, 10 m, and 30 m outside the solid coal slope of the channel, the starting distances for the increase in stress caused by mining are 100 m, 40 m, and 20 m, respectively. At the same time, there are significant differences in the vertical stress peaks at different positions of the solid coal. At 1 m, 10 m, and 30 m of the solid coal slope, the stress peaks after penetration are 60 MPa, 40 MPa, and 20 MPa, respectively. As the distance between the monitoring position and the retracement channel of the solid coal slope increases, the stress peak gradually decreases, indicating that the deep surrounding rock outside the solid coal is less affected by mining.

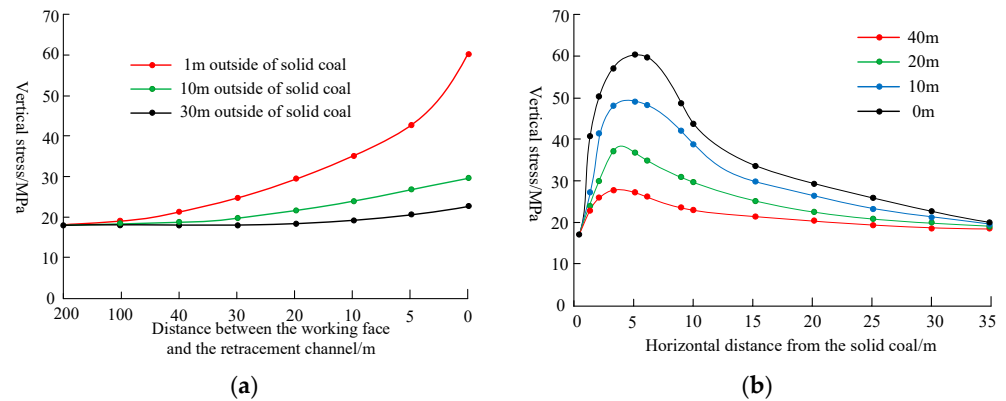


Figure 7. Stress analysis at the solid coal slope of the retracement channel. (a) Curve of stress variation with mining at different positions outside the solid coal slope. (b) Stress distribution of solid coal outside the retracement channel.

Figure 7b shows the stress distribution of solid coal outside the retracement channel at different mining distances. From the figure, it can be seen that the vertical stress of the solid coal in the retracement channel is distributed in a single peak form, and the peak stress continuously increases with the mining of the working face. When the working face is connected to the retracement channel, the stress reaches its maximum, and the peak stress reaches above 60 MPa at a distance of 5 m from the surface in the shallow part of the solid coal slope.

3.3. Deformation and Failure Characteristics of Surrounding Rock in the Retracement Channel

The deformation and failure characteristics of the surrounding rock of the retracement channel under different simulation schemes are shown in Figure 8.

Based on the comprehensive analysis of the above displacement cloud map, it can be seen that the changes in the surrounding rock of the retracement channel are distributed in three stages: in the first stage, the working face is far from the retracement channel, and at this time, the retracement channel is basically not affected by mining, and the deformation of the surrounding rock is very small. In the second stage, when the working face is withdrawn to a certain distance from the retracement channel, it is gradually affected by the overburden of the adjacent goaf, and the deformation of the surrounding rock begins to increase significantly. In the third stage, the working face is about to connect with the retracement channel, and at this time, the retracement channel is most severely affected by mining, and the surrounding rock deformation and damage are obvious, with a sharp increase in deformation.

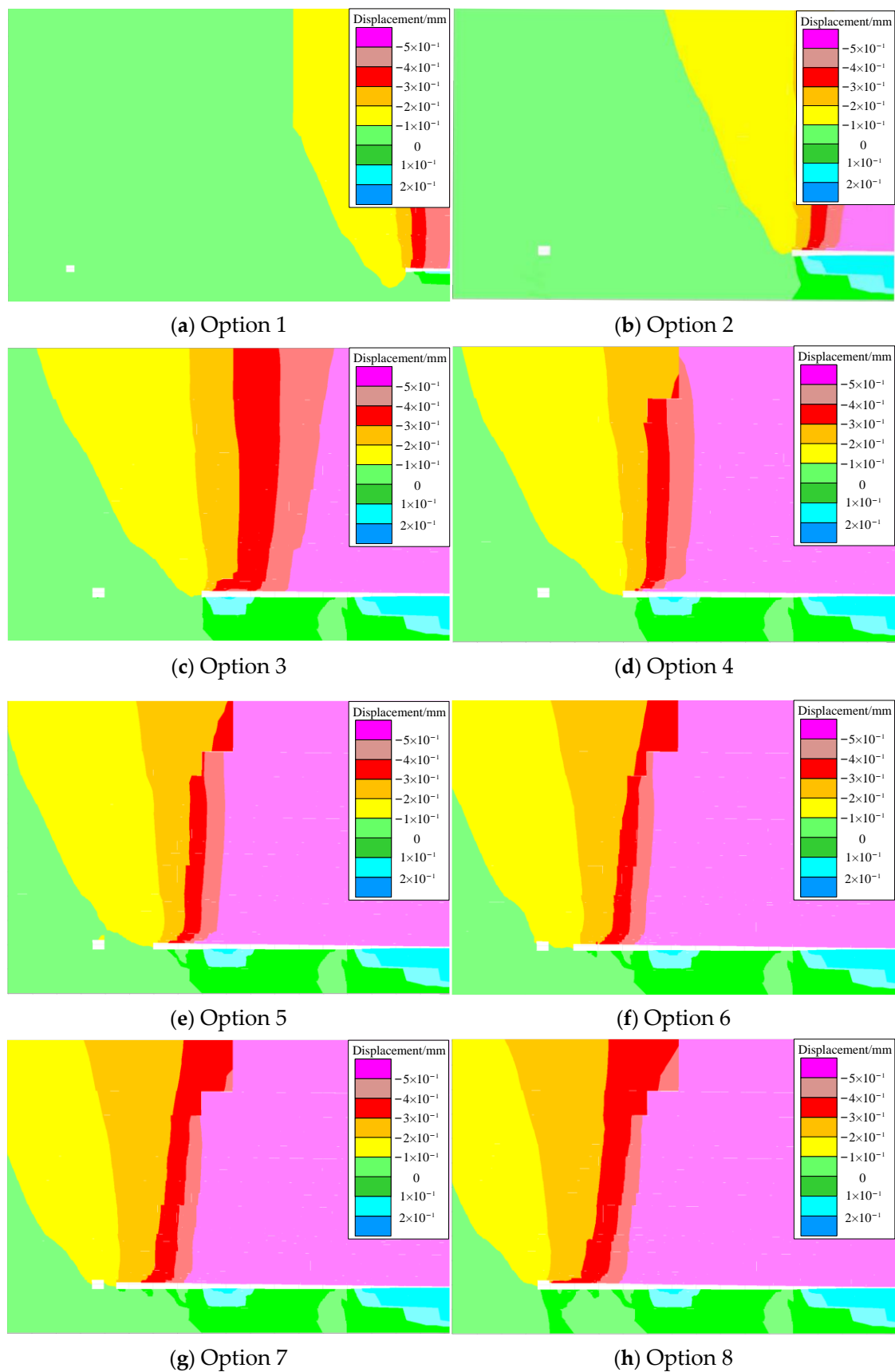


Figure 8. Displacement cloud map of the working face at different distances from the retracement channel.

From Figure 9, it can be seen that the deformation law of the roof of the retracement channel is basically consistent with the deformation law of the side. The two-sides convergence of the retracement channel at the same section is greater than the roof convergence. When the working face is 30 m away from the retracement channel, it is less affected by mining, and the deformation of the surrounding rock can be ignored. When the working face is 5–30 m away from the retracement channel, it begins to increase due to the influence of mining, and the remaining coal body of the working face is affected by the bending and sinking of the overburden. The energy accumulated in the surrounding rock increases, and the cumulative deformation of the roof and two sides reaches 50 mm and 100 mm, respectively. When the working face is 0–5 m away from the retracement channel, the deformation of the surrounding rock of the retracement channel increases sharply, with the cumulative deformation of the roof and two sides reaching 320 mm and 450 mm, respectively, exceeding the maximum allowable caving height of the retracement channel by 300 mm.

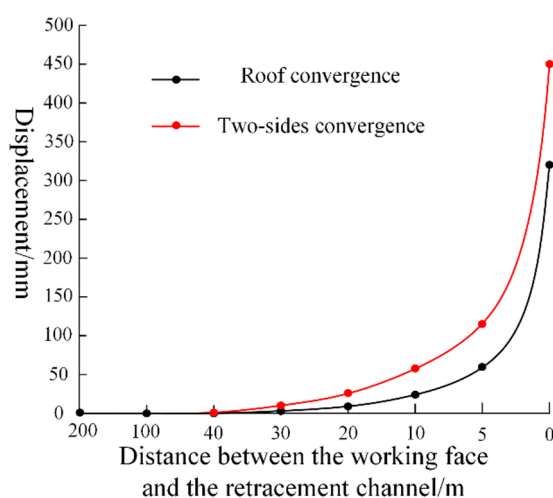


Figure 9. Deformation curve of surrounding rock in the retracement channel under the original support conditions.

4. Mechanism of Deformation and Failure of Surrounding Rock in the Retracement Channel and Design of Reinforcement Support

4.1. Analysis of the Surrounding Rock Structure of the Retracement Channel

4.1.1. State of the Overburden Structure of the Retracement Channel

According to the theory of masonry beams, the main roof is at the breaking step distance. As the working face advances, the rock blocks collapse and are arranged neatly, and the friction force between them can form a semi-arch structure [40,41]. After mining in the 360808 working face, the roof collapsed and broke on the side of the coal pillar in the lower section. A typical mechanical model was analyzed to determine the three different fracture positions after the main roof of the end zone broke [42,43], as shown in Figure 10.

From the fracture state of the 360808 working face, it can be seen that the studied fracture morphology is more in line with the second type; that is, the main roof fracture is above the retracement channel, as shown in Figure 10b. The load-bearing capacity of the overburden in the retracement channel increases. The immediate roof and hydraulic support at the roof of the retracement channel bear most of the load of the fractured block B. The physical coal slope undergoes tensile deformation under the influence of dynamic pressure, and the roof on the side of the retreat slope sinks significantly. When the bearing capacity reaches its limit, a fracture occurs immediately near the coal wall and above the coal pillar of the solid coal, leading to a sharp decrease in its bearing capacity. Therefore, the deformation of the retracement channel is relatively large, and it is more crucial to strengthen the maintenance of the roof at this time.

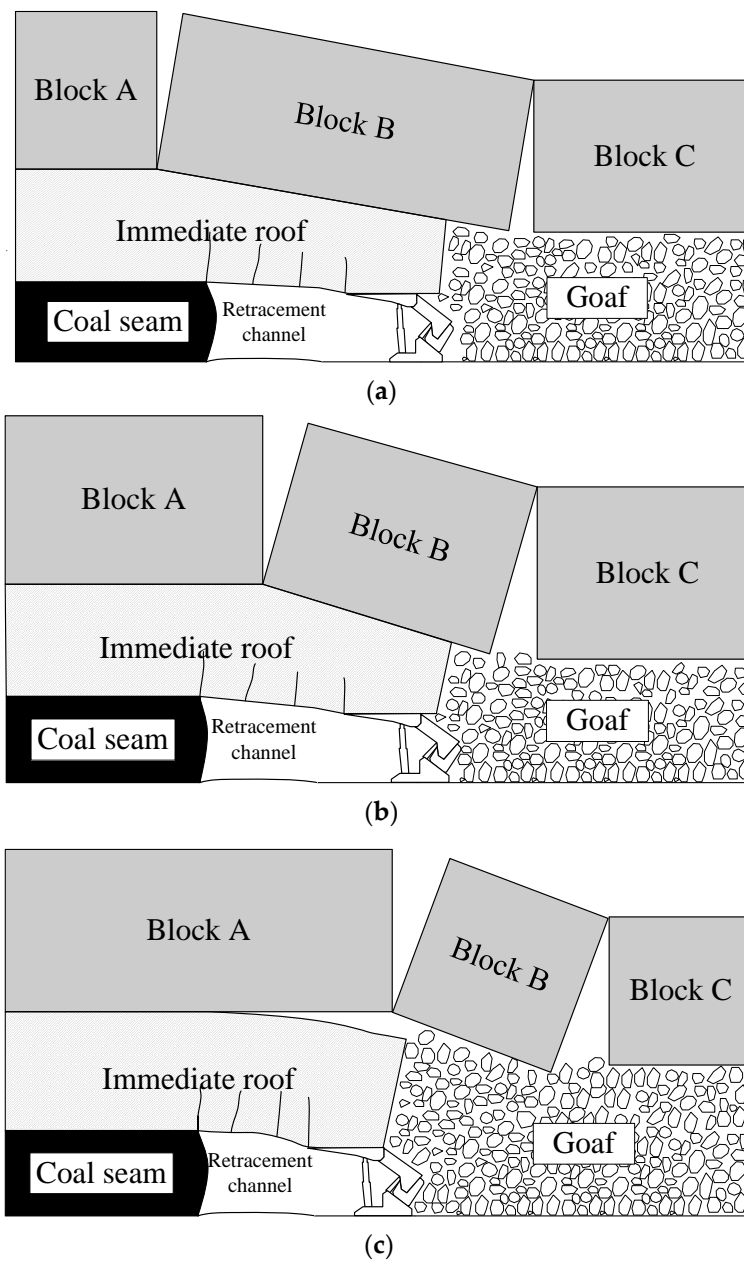


Figure 10. Overburden structure of the working face. (a) The fracture location is above the coal seam. (b) The fracture is located on the upper part of the retrace channel. (c) The fracture is located on the side of the goaf.

4.1.2. Mechanism of Surrounding Rock Failure in the Retracement Channel

- (1) When the working face is far from the retracement channel, the remaining width of the coal pillar between the working face and the retracement channel is large, and it will not be affected by the mining of the working face. The integrity of the roof and the surrounding rock on the two sides is suitable, and the surrounding rock is in a stable state. During the final mining period, as the working face advances, the width of the interval coal between the working face and the retracement channel continuously decreases, forming a gradually changing width coal pillar. During the connection process between the retracement channel and the working face, there is a significant trend of surrounding rock deformation and stress increase. The gradient coal pillar is affected by the superposition of advanced support pressure and lateral support stress

of the retracement channel, and it fails when it exceeds the strength limit. The shallow plastic failure range of the gradient coal pillar expands, as shown in Figure 11.

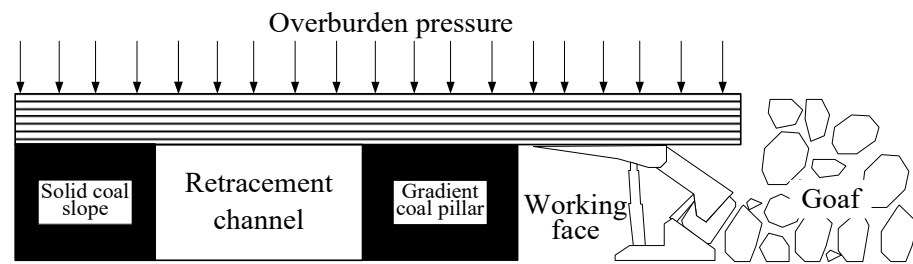


Figure 11. Schematic diagram of mining before the connection between the working face and the retracement channel.

- (2) After the connection between the working face and the retracement channel, the advanced support pressure of the working face begins to transfer to the protective coal pillar outside the retracement channel. The deformation and pressure of the surrounding rock inside the retracement channel both increase sharply, and the roof significantly sinks, expanding the range of solid coal slope fragmentation.

From the above analysis, it can be concluded that the dynamic pressure linkage effect caused by the unstable deformation of the gradient coal pillar and the unreasonable position of the main roof fracture during the connection between the working face and the retracement channel is the fundamental reason for the catastrophic instability of the surrounding rock of the retracement channel.

4.2. Construction of Instability Criteria

When the main roof fracture occurs above the retracement channel, due to the absence of coal below the fracture line to bear the end load of the fracture block, one end of the main roof fracture acts on the immediate roof above the retracement channel, and the other end is carried by the gangue in the goaf [44]. At this time, the immediate roof is subjected to the superposition effect of the overburden pressure and the pressure of the key block and its overburden behind the main roof, which has a significant impact on the retracement channel. The surrounding rock undergoes significant deformation under stress, and the stress analysis of the surrounding rock is shown in Figure 12.

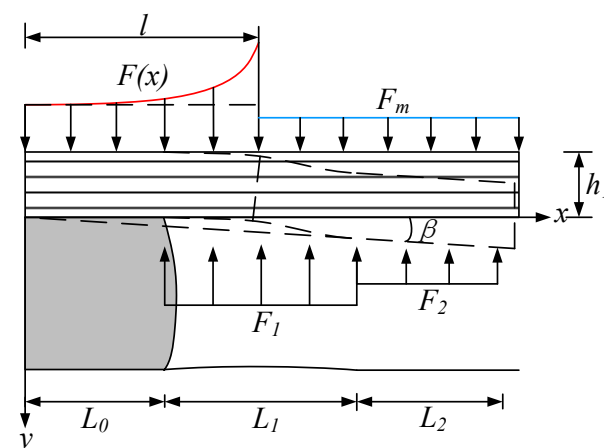


Figure 12. Analysis of the stress on surrounding rock when the main roof fractures above the retracement channel.

According to the force analysis diagram, it can be seen that the upper part of the cantilever rock beam in the retracement channel is mainly affected by the overburden pressure $F(x)$ and the pressure F_m of the rear main roof key block and its overburden. The

internal support body support force F_1 and the working face shield support force F_2 play an upward supporting role on the rock beam.

The main uniformly distributed force $F(x)$ above the cantilever rock beam can be expressed as the advanced support pressure [45]:

$$F(x) = (m - 1)\gamma H e^{-\frac{2f\mu}{M}(l-x)} + \gamma H \quad (1)$$

where m represents the stress concentration coefficient of the roof, γ represents the unit weight of the overburden, H represents the burial depth of the overburden, f represents the coefficient of friction, μ represents the lateral pressure coefficient, M represents the mining height, and l represents the main roof fracture position.

From the deflection curve equation of a cantilever beam under a uniformly distributed load, it can be seen that [46]

$$L(x) = \frac{qx^2}{24EI} \left[x^2 - 4x(L_0 + L_1 + L_2) + 6(L_0 + L_1 + L_2)^2 \right] \quad (2)$$

where E represents the immediate roof elastic modulus, I represents the immediate roof section moment of inertia, L_0 represents the length of the solid coal slope immediately penetrated by the roof, L_1 represents the width of the retracement channel, and L_2 represents the roof control distance of the working face bracket.

When the main roof fractures above the retracement channel, the deformation of the immediate roof is closely related to the rotational sinking of the broken main roof rock block. Regarding the movement law of the surrounding rock, when the main roof fractures above the retracement channel, the immediate roof is regarded as a deformed body, which is supported by anchor cables and individual pillars. According to the principle of energy conservation, the rotational deformation work of the main roof rock block is equal to the work performed by external support forces such as anchor cables and individual pillars. Therefore, it is necessary to solve the main roof, immediate roof, and support work separately.

(1) Main roof key block rotation sinking work.

When considering the rotation and sinking of the main roof, the work performed by the main roof to the immediate roof is as follows:

$$W_1 = \int_l^{L_0+L_1+L_2} F_m \theta x dx = \frac{\gamma_0 h_m \theta \left[(L_0 + L_1 + L_2)^2 - l^2 \right]}{2} \quad (3)$$

where θ represents the sinking angle of the key block rotation, γ_0 represents the main unit weight of the roof rock mass, and h_m represents the thickness of the key block and its overburden.

(2) Work immediately against self-weight.

Under the influence of the key block's rotational sinking, the immediate roof will also undergo rotational sinking, and its center of gravity will change. When the immediate jacking angle is β , according to the geometric relationship of the immediate jacking sinking analyzed in reference [47], it can be seen that the vertical displacement of the center of gravity of the immediate jacking under the rotation of the key block is as follows:

$$S_0 = \frac{1}{2} [h_1(1 - \cos \beta) - \sin \beta(L_0 + L_1 + L_2 - l)] \quad (4)$$

Therefore, the immediate roof work is as follows:

$$W_2 = -\frac{1}{2} \gamma_1 h_1 (L_0 + L_1 + L_2 - l) [\sin \beta(L_0 + L_1 + L_2 - l) - h_1(1 - \cos \beta)] \quad (5)$$

where γ_1 represents the bulk density of the immediate roof rock mass.

(3) Work performed by the internal support body of the retracement channel.

When the immediate roof of the retracement channel sinks, the support strength of the internal support body is F_1 , and the work performed by the internal support body is as follows:

$$W_3 = \int_l^{L_0+L_1} \frac{F_1}{L_0 + \frac{L_1}{2}} S_1 dx = \frac{F_1 S_1 [(L_0 + L_1)^2 - l^2]}{2L_0 + L_1} \quad (6)$$

where S_1 represents the sinking amount in the middle of the roof of the retracement channel.

(4) Work performed by hydraulic support with cover on the working face.

When the main roof rotates, the overburden exerts pressure on the retracement channel. The shield hydraulic support of the working face, to some extent, blocks the rotation deformation of the main roof and works on the immediate roof. The support strength of the shield hydraulic support is F_2 , and the work performed by the shield hydraulic support is as follows:

$$W_4 = \int_{L_0+L_1}^{L_0+L_1+L_2} \frac{F_2 x}{L_0 + \frac{L_1}{2}} S_1 dx = \frac{F_2 S_1 [(L_0 + L_1 + L_2)^2 - (L_0 + L_1)^2]}{2L_0 + L_1} \quad (7)$$

(5) Strain energy of the solid coal slope of the retracement channel.

Under the rotary sinking effect of the main roof key block, the strain energy of the coal body affected by the immediate compression and retracement of the solid coal slope of the channel is as follows:

$$W_5 = \int_0^{L_0} \zeta \left(\frac{S_1 x}{L_0 + \frac{L_1}{2}} \right)^2 dx = \frac{\zeta S_1^2 L_0^3}{3 \left(L_0 + \frac{L_1}{2} \right)^2} \quad (8)$$

where ζ represents the stiffness coefficient of the solid coal slope.

(6) Immediate roof strain energy.

Immediately jacking the rock mass generates compressive strain energy due to compression, namely:

$$W_6 = \frac{\zeta S_1^2 h_1 L_0^3}{4E \left(L_0 + \frac{L_1}{2} \right)^2} \quad (9)$$

The above formulas are applicable to the condition of hard roofs. After the working face is connected with the retracement channel, the energy release of the roof above the channel and the energy accumulation of the internal structure of the channel during the breaking process of the roof, quantifying the energy transmission process, intuitively reflecting the movement state of the overburden, and establishing a foundation for the construction of structural instability criteria. However, the above mechanical model regards the main roof block as a standard block with constant stiffness, ignores the deformation of the block itself, and does not consider the influence of fracture line angle on the energy transfer law of the structure.

According to energy conservation, when the external energy is equal to the internal energy consumption, the surrounding rock of the retracement channel is in a critical equilibrium state. If the ratio of external work to internal energy consumption is k , then there is as follows:

$$k = \frac{W_1 + W_2}{W_3 + W_4 + W_5 + W_6} \quad (10)$$

At this point, it can be divided into two states:

$$\begin{cases} \textcircled{1} \text{When } k \leq 1, \text{ the surrounding rock loses stability} \\ \textcircled{2} \text{When } k > 1, \text{ the surrounding rock keeps stability} \end{cases}$$

When the sum of external energy is greater than the sum of internal energy consumption, the surrounding rock of the retracement channel becomes unstable.

4.3. Strengthening Support Strength and Timely Machine Determination

4.3.1. Strengthening Support Strength Design

When the energy of the surrounding rock in the retracement channel is in equilibrium, the minimum safe support strength F_1 can be obtained by bringing the above Formulas (1) to (10) into $W_1 + W_2 = W_3 + W_4 + W_5 + W_6$:

$$F_1 = \frac{W_3(2L_0 + L_1)}{S_1[(L_0 + L_1)^2 - l^2]} \quad (11)$$

When the support force F_2 of the shield support in the working face is constant, according to the actual mining requirements, the maximum value S_{\max} of the roof caving in the working face can be determined, which is the maximum value of S_1 . At this time, the minimum support strength F_{\min} of the internal support body corresponding to the maximum caving degree can be obtained. Due to different geological conditions and the stability of the support body, the calculation of the minimum safety support strength $F_{1\min}$ should take a certain safety coefficient $\eta = 1.2$, and then $F_{1\min} = 1.2F_{\min}$.

4.3.2. Timing of Strengthening Support

According to the deformation and failure characteristics of the surrounding rock of the retracement channel, when the working face is 5–30 m away from the retracement channel, it begins to increase under the influence of mining. In the retracement channel, the surrounding rock begins to deform, and the sinking rate shows an increasing trend. When the working face is 0–5 m away from the retracement channel, the deformation of the surrounding rock in the retracement channel increases sharply, and the subsidence of the roof and the rate of the two sides moving in significantly increase. When the working face is 5 m away from the retracement channel, the roof subsidence reaches $\Delta_1 = 50$ mm, which is the critical point for the sudden change in roof subsidence rate. Therefore, the timing for strengthening support before the working face is 5 m away from the retracement channel.

Based on a comprehensive analysis of the selection method for strengthening support under similar engineering conditions [48], a certain safety coefficient $\eta_a = 0.8$ is taken here to calculate the maximum safe settlement $\Delta_2 = \eta_a \Delta_1 = 40$ mm. Based on the curve of the subsidence of the roof of the retracement channel in Figure 10, it can be seen that the corresponding working face is 15 m away from the retracement channel at this time. Therefore, the timing for strengthening support is at a distance of 15 m from the working face to the retracement channel.

4.3.3. Strengthening Support Methods

The original support method is shown in Figure 4. Under the original support conditions, the support strength is not sufficient to maintain the stability of the retracement channel structure. In the final mining period of the 360808 working face, in order to achieve a safe connection between the working face and the retracement channel, measures such as anchor reinforcement are considered to strengthen support for the retracement channel.

In order to prevent large-scale overall falling off the roof rock layer of the roadway, a “composite arch” reinforced with anchor cables is used. The “suspension beam” theory is used to suspend the entire structure in a hard main roof, and the falling method is considered based on the most severe falling height greater than the length of the anchor rod [49]. Under the condition of neglecting the cohesive force and internal friction force of the rock mass, the equilibrium of the vertical force is taken, and the anchor cable parameters are calculated as follows:

Calculation of anchor cable length:

$$M = M_a + M_b + M_c + M_d \quad (12)$$

where M represents the total length of the anchor cable, and M_a , M_b , M_c , and M_d represent the anchoring length of the anchor cable penetrating into a relatively stable rock layer, the thickness of unstable rock layers that need to be suspended, the thickness of the upper tray and anchor, the required exposed stretching length.

The anchoring length L_a of the anchor cable is determined by the following formula:

$$M_a \geq \phi \cdot d_1 \cdot f_a / (4 \cdot f_c) \quad (13)$$

where ϕ represents the safety factor, d_1 represents the diameter of the anchor cable steel strand, f_a represents the tensile strength of the steel strand, and f_c represents the anchoring adhesion of the anchor cable.

Calculation of anchor cable spacing:

$$c = n \cdot F / (2 \cdot B_a \cdot H_a \cdot \gamma) \quad (14)$$

where c represents the spacing of anchor cables, n represents the number of anchor cables in each row, F represents the ultimate bearing capacity of the anchor cable, B_a represents the maximum caving width of the roadway, H_a represents the height of roadway collapse, and γ represents the bulk density of the rock mass.

Number of anchor cables per row:

$$N = \phi \cdot G / F \quad (15)$$

where N represents the number of anchor cables in each row and G represents the self-weight of the suspended rock.

5. Field Practice Verification

5.1. Parameter Analysis and Calculation

5.1.1. Energy Balance Calculation

(1) Calculation of channel support strength under original support conditions.

When the overburden on the retracement channel of the 360808 working face breaks above the roof, the key block's rotational sinking angle θ is 5° , and rock mass density $\gamma_0 = 25 \text{ kN/m}^3$. The thickness of the key block and its adjacent overlying strata is selected with reference to the height of the collapse zone and fracture zone, $h_m = 54 \text{ m}$. The length of immediate roof penetration into the solid coal slope $L_0 = 1.94 \text{ m}$. The width of the retracement channel $L_1 = 5.2 \text{ m}$. The roof control distance of the working face support $L_2 = 5.0 \text{ m}$. The main roof fracture position $l = 4.54 \text{ m}$. Immediate roof thickness $h_1 = 5 \text{ m}$. Immediate return angle $\beta = 3^\circ$. The subsidence in the middle of the roof convergence of the retracement channel $S_1 = 320 \text{ mm}$. The stiffness coefficient of the solid coal slope $\zeta = 10 \text{ MPa/m}$. The stiffness coefficient of the immediate roof rock layer $\zeta_1 = 50 \text{ MPa/m}$.

When the energy of the surrounding rock in the retracement channel is in equilibrium, the above parameters are taken into Equation (11), and the calculation shows that the internal support strength F_1 at this time is $F_1 = 2041 \text{ kN/m}$

(2) Calculation of minimum safety support strength.

When the sinking amount in the middle of the roof of the retracement channel reaches the maximum allowable value for roof caving, $S'_1 = 300 \text{ mm}$.

At this point, the minimum safety support strength F'_1 is as follows:

$$F'_1 = 2374.89 \text{ kN/m}$$

Due to the influence of different geological conditions and the stability of the support body, the calculation of safety support strength $F_{1\min}$ should take a certain safety coefficient $\eta = 1.2$, where $F_{1\min} = 1.2F'_1 = 2849.87$ kN/m.

Based on a comprehensive analysis of the strength of the support under the two support conditions mentioned above, it can be calculated that the support strength that should be provided for strengthening the support design is $F_Z = F_{1\min} - F_1 = 809$ kN/m.

5.1.2. Strengthening Support Plan

In the original method, the support strength provided by anchor cable support was 423 kN/m. To meet the safety support strength, the support strength provided by the anchor cable should reach 1232 kN/m. It is planned to add a row of anchor cables every 1600 mm along the channel roof, with a length of 7.2 m, and the number of anchor cables in each row is unchanged. The plan verification is as follows:

Selection of anchor cable material: Select 1 × 19 S, $\Phi = 21.8$ mm prestressed steel strand production.

The thickness of unstable rock layers that need to be suspended is taken as the immediate roof thickness $M_b = 5$ m. The thickness of the upper tray and anchor is $M_c = 0.1$ m. The required exposed stretching length $M_d = 0.25$ m. Safety coefficient $\phi = 2$. Anchor cable steel strand diameter $d_1 = 21.8$ mm. Steel strand tensile strength $f_a = 1860$ N/mm². The anchoring adhesion of the anchor cable $f_c = 10$ N/mm². Number of anchor cables per row $n = 5$. The bearing capacity of the steel strand is taken as $F = 583$ kN.

According to Formula (13), $M_a \geq 1621.92$ mm can be calculated as $M_a = 1.7$ m. The length of the anchor cable can be calculated by Formula (12) as $M \geq 7.05$ m. Based on the calculation results, the selected anchor cable length is 7.2 m, which meets the requirements.

The anchor cable spacing can be calculated by Formula (14) as $c = 1.802$ m. According to the calculation results, the selected anchor cable spacing of 1.6 m is less than the calculated value of 1.802 m, which meets the requirements.

The number of anchor cables in each row can be calculated by Formula (15) to obtain $N = 2.775$ m. Based on the calculation results, five anchor cables are taken from each row to meet the requirements.

According to suspension theory calculation, the use of anchor cables $\Phi 21.8$ mm × 7200 mm prestressed steel strand anchor cable with a spacing of 1200 × 1200 mm, 5 in each row, arranged perpendicular to the roof of the roadway, as shown in Figure 13.

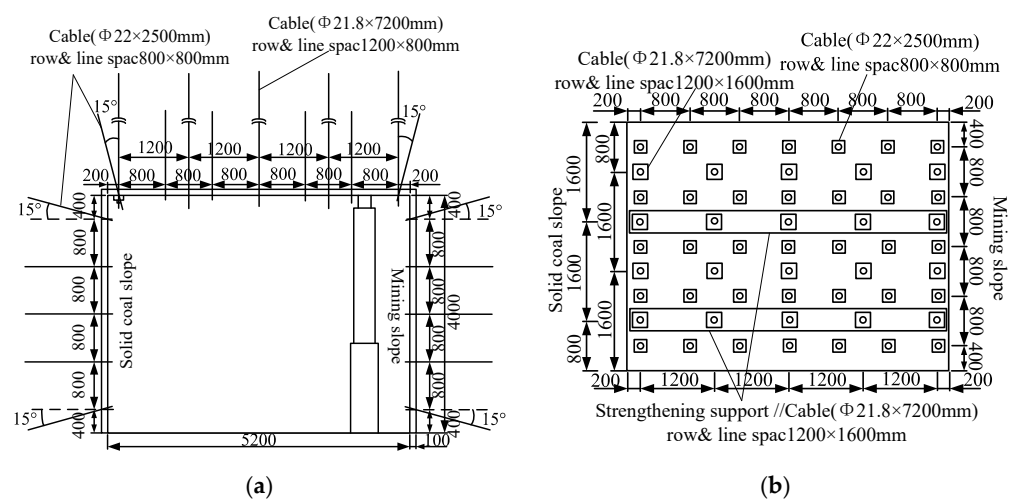


Figure 13. Schematic diagram of reinforced support status. (a) Cross-section of channel direction. (b) Top view.

5.2. Analysis of Strengthening Support Effect

5.2.1. Strengthen the On-Site Effect of Support

During the initial mining of the working face, the retracement channel was not affected by mining, and the deformation of the surrounding rock in the roadway was very small. However, as the mining approached the stop line, the retracement channel became more significantly affected by mining, and the degree of deformation and damage to the surrounding rock intensified. The roof significantly sank, and the deformation of the two sides significantly squeezed toward the interior of the channel. As shown in Figure 14, the deformation of the surrounding rock in the retracement channel is large, and the anchor rods and cables in the tunnel are damaged and ineffective. There are also accidents of hydraulic support and stack support pressing in the retracement channel, which seriously affect the safe retracement and rapid movement of the working face. After strengthening the support of the retracement channel by adding anchor cables, the degree of deformation and damage to the surrounding rock is reduced, and there is no significant deformation or concentrated fragmentation in the area, indicating a significant support effect.

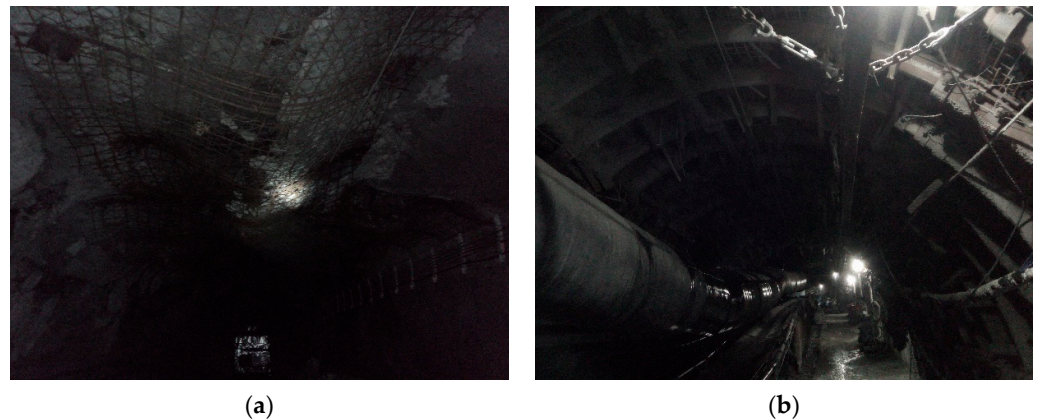


Figure 14. Schematic diagram of deformation comparison of the withdrawal channel before and after strengthening support. (a) Before strengthening support. (b) After strengthening support.

5.2.2. Analysis of On-Site Monitoring Results

According to the deformation and failure characteristics of the surrounding rock in the retracement channel, the part with a large amount of deformation in the retracement channel is located in the middle section. Therefore, monitoring points are arranged in the middle of the retracement channel to monitor the deformation of the surrounding rock under the strengthened support plan.

According to the deformation curve of the surrounding rock in Figure 15, it can be seen that after strengthening the support, the position of the measuring point in the working face 20 m away from the retracement channel is very little affected by mining, and the deformation amount and deformation rate of the surrounding rock can be ignored. When the mining face reaches a distance of 15 m from the retracement channel, the deformation amount and rate of surrounding rock begin to increase. During the distance of 5 m between the working face and the retracement channel and the connection period, the roof convergence and the two-sides convergence reached 230 mm and 310 mm, respectively. Under the effect of strengthening support, the two decreased by 90 mm and 140 mm, respectively, meeting the deformation requirements of the channel, and the support effect is significant.

Based on the comprehensive analysis of the above deformation curves, it can be concluded that strengthening support can effectively improve the stability of surrounding rock. Under the action of strengthening support, the deformation rate of the surrounding rock before and after the connection decreased significantly, and the deformation of the surrounding rock before and after the connection was effectively controlled, resulting in a suitable support effect.

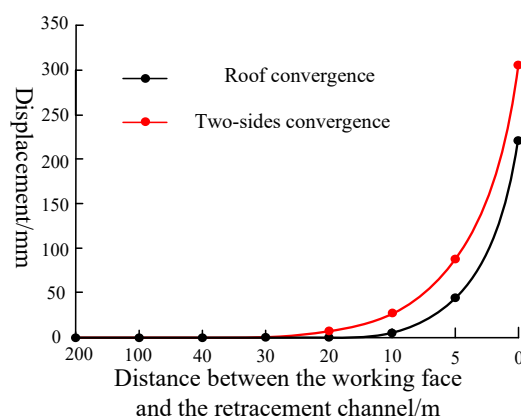


Figure 15. Deformation curve of surrounding rock in the retracement channel.

6. Conclusions

In response to the problem of controlling the surrounding rock of the retracement channel in the 360808 working face of Xinji No. 1 Mine, numerical simulation, theoretical analysis, and on-site monitoring were comprehensively used to systematically analyze the mechanism of large deformation and failure of the surrounding rock of the retracement channel, as well as the stress distribution law of the solid coal in the retracement channel. Based on this, the timing and parameter design of strengthening support for the retracement channel in the final mining stage of the working face was proposed. The main conclusions were as follows:

- (1) A gradual excavation model for the working face under the super-thick nappe was established, and the peak stress of the surrounding rock in the retracement channel during the final mining stage was obtained as the mining face continued to increase. It was found that the two sides of the coal pillars in the retracement channel began to exhibit asymmetric deformation characteristics when the width of the gradually changing coal pillars in the working face decreased to 30 m.
- (2) A mechanical analysis model of the surrounding rock was established when the basic roof ruptured above the retracement channel. The criterion for instability of surrounding rock was obtained from an energy perspective, and a strengthening support method of adding anchor cables was proposed. The timing for strengthening support was determined to be when the working face was withdrawn to a distance of 15 m from the retracement channel.
- (3) Through on-site real-time monitoring, it was found that the numerical simulation results were consistent with the actual situation. After adopting strengthened support, the subsidence of the roof was reduced by 90 mm, and the displacement of the two sides was reduced by 140 mm, both of which met the deformation requirements of the retracement channel. The support effect was significant.

Author Contributions: Conceptualization, R.Z., X.Y., X.L. (Xuesheng Liu) and X.L. (Xuebin Li); methodology, X.L. (Xuesheng Liu), Y.G. and X.L. (Xuebin Li); software, X.L. (Xuesheng Liu), Y.G. and X.L. (Xuebin Li); validation, R.Z., X.Y. and K.W.; formal analysis, Y.G., X.L. (Xuebin Li) and C.X.; investigation, R.Z., X.Y. and C.X.; resources, K.W., X.L. (Xuesheng Liu) and R.Z.; data curation, R.Z., X.Y., K.W. and Y.G.; writing—original draft preparation, Y.G., X.L. (Xuebin Li) and C.X.; writing—review and editing, R.Z., X.Y., X.L. (Xuesheng Liu) and K.W.; visualization, Y.G., X.L. (Xuebin Li) and C.X.; supervision, R.Z. and X.L. (Xuesheng Liu); project administration, X.Y. and K.W.; funding acquisition, R.Z., X.Y., X.L. (Xuesheng Liu) and K.W. All authors have read and agreed to the published version of the manuscript.

Funding: The research described in this paper was financially supported by the National Natural Science Foundation of China (Nos. 52174122, 52374218), Excellent Youth Fund of Shandong Natural Science Foundation (No. ZR2022YQ49), Taishan Scholar in Shandong Province (tsqn202211150), and the Engineering Research Center of Geothermal Resources Development Technology and Equipment, Ministry of Education, Jilin University.

Institutional Review Board Statement: Not applicable.

Informed Consent Statement: Not applicable.

Data Availability Statement: Data are contained within the article.

Acknowledgments: We thank Cao Anye of China University of Mining and Technology for his support and help with this paper.

Conflicts of Interest: The authors declare no conflict of interest.

References

1. Tan, N.; Yang, R.; Tan, Z. Influence of complicated faults on the differentiation and accumulation of in-situ stress in deep rock mass. *Int. J. Miner. Met. Mater.* **2023**, *30*, 791–801. [\[CrossRef\]](#)
2. Zhang, B.; Zhou, H.; Chang, Q.; Zhao, X.; Sun, Y. The Stability Analysis of Roadway near Faults under Complex High Stress. *Adv. Civ. Eng.* **2020**, *2020*, 8893842. [\[CrossRef\]](#)
3. Li, X.; Liu, X.; Tan, Y.; Chen, A.; Wang, H.; Wang, X.; Yang, S. Rheological mechanical properties and its constitutive relation of soft rock considering influence of clay mineral composition and content. *Int. J. Coal Sci. Technol.* **2023**, *10*, 48. [\[CrossRef\]](#)
4. Xie, S.; Wang, E.; Chen, D.; Li, H.; Jiang, Z.; Yang, H. Stability analysis and control technology of gob-side entry retaining with double roadways by filling with high-water material in gently inclined coal seam. *Int. J. Coal Sci. Technol.* **2022**, *9*, 52. [\[CrossRef\]](#)
5. Shan, R.; Li, Z.; Wang, C.; Wei, Y.; Bai, Y.; Zhao, Y.; Tong, X. Research on the mechanism of asymmetric deformation and stability control of near-fault roadway under the influence of mining. *Eng. Fail. Anal.* **2021**, *127*, 105492. [\[CrossRef\]](#)
6. Yao, N.; Wang, Y.; Yao, Y.; Song, H.; Wang, L.; Peng, T.; Sun, X. Progress of drilling technologies and equipment for complicated geological conditions in underground coal mines in China. *Coal Geol. Explor.* **2020**, *48*, 2.
7. Liu, X.; Song, S.; Tan, Y.; Fan, D.; Ning, J.; Li, X.; Yin, Y. Similar simulation study on the deformation and failure of surrounding rock of a large section chamber group under dynamic loading. *Int. J. Min. Sci. Technol.* **2021**, *31*, 495–505. [\[CrossRef\]](#)
8. Elizalde, C.; Griffith, W.A.; Miller, T. Thrust fault nucleation due to heterogeneous bedding plane slip: Evidence from an Ohio coal mine. *Eng. Geol.* **2016**, *206*, 1–17. [\[CrossRef\]](#)
9. Liu, X.; Fan, D.; Tan, Y.; Ning, J.; Song, S.; Wang, H.; Li, X. New detecting method on the connecting fractured zone above the coal face and a case study. *Rock Mech. Rock Eng.* **2021**, *54*, 4379–4391. [\[CrossRef\]](#)
10. Jiang, F.X.; Wei, Q.D.; Wang, C.W.; Yao, S.L.; Zhang, Y.; Han, R.J.; Wei, X.Z.; Li, Z.C. Analysis of rock burst mechanism in extra-thick coal seam controlled by a huge thick conglomerate and thrust fault. *J. China Coal Soc.* **2014**, *39*, 1191–1196.
11. Gao, X.; Li, Y.; Zhang, Z.; Zhang, Z.; Yu, H.; Huang, Z.; Yue, C. Prevention and control technology of large deformation double active advance blasting pre-cracking roof in soft rock tunnels. *J. Coal Ind.* **2020**, *45* (Suppl. S2), 589–598.
12. Li, C.; Zhang, Y.; Zhang, G.; Gao, S.; Zhang, H. The stress evolution and crack propagation mechanism of the bottom plate under dynamic disturbance in deep mining. *J. Geotech. Eng.* **2018**, *40*, 2031–2040.
13. Batugin, A.; Wang, Z.; Su, Z.; Sidikovna, S.S. Combined support mechanism of rock bolts and anchor cables for adjacent roadways in the external staggered split-level panel layout. *Int. J. Coal Sci. Technol.* **2021**, *8*, 659–673. [\[CrossRef\]](#)
14. Tan, Y.L.; Fan, D.Y.; Liu, X.S.; Song, S.L.; Li, X.F.; Wang, H.L. Numerical investigation on failure evolution of surrounding rock for super-large section chamber group in deep coal mine. *Energy Sci. Eng.* **2019**, *7*, 3124–3146. [\[CrossRef\]](#)
15. Liu, X.; Fan, D.; Tan, Y.; Song, S.; Li, X.; Ning, J.; Gu, Q.; Ma, Q. Failure evolution and instability mechanism of surrounding rock for close-distance parallel chambers with super-large section in deep coal mines. *Int. J. Geomech.* **2021**, *21*, 04021049. [\[CrossRef\]](#)
16. Wu, Q.; Jiang, L.; Wu, Q. Study on the law of mining stress evolution and fault activation under the influence of normal fault. *Acta Geodyn Geomater* **2017**, *14*, 357–369. [\[CrossRef\]](#)
17. Jiao, Z.; Jiang, Y.; Zhao, Y.; Zhang, M.; Hu, H. Study on the dynamic mechanical response characteristics of working faces passing through faults. *J. China Univ. Min. Technol.* **2019**, *48*, 54–63.
18. Islam, M.R.; Shinjo, R. Mining-induced fault reactivation associated with the main conveyor belt roadway and safety of the Barapukuria coal mine in Bangladesh: Constraints from BEM simulations. *Int. J. Coal Geol.* **2009**, *79*, 115–130. [\[CrossRef\]](#)
19. Li, C.; Guo, X.F.; Huo, T.H.; Liu, R. Coal pillar design of pre-excavated double equipment withdrawal channel and its surrounding rock stability control. *J. Huazhong Univ. Sci. Technol. (Nat. Sci. Ed.)* **2021**, *49*, 20–25+31.
20. Qin, B.; He, F.; Zhang, X.; Xu, X.; Wang, W.; Li, L.; Dou, C. Stability and Control of Retracement Channels in Thin Seam Working Faces with Soft Roof. *Shock Vib.* **2021**, *2021*, 8667471. [\[CrossRef\]](#)
21. Ma, J.; Guan, J.; Duan, J.; Huang, L.; Liang, Y. Stability analysis on tunnels with karst caves using the distinct lattice spring model. *Undergr. Space* **2021**, *6*, 469–481. [\[CrossRef\]](#)
22. Zhang, F.; Cui, L.; An, M.; Elsworth, D.; He, C. Frictional stability of Longmaxi shale gouges and its implication for deep seismic potential in the southeastern Sichuan Basin. *Deep Undergr. Sci. Eng.* **2022**, *1*, 3–14. [\[CrossRef\]](#)
23. Kong, P.; Jiang, L.; Shu, J.; Wang, L. Mining stress distribution and fault-slip behavior: A case study of fault-influenced longwall coal mining. *Energies* **2019**, *12*, 2494. [\[CrossRef\]](#)
24. Han, Z.; Li, D.; Li, X. Dynamic mechanical properties and wave propagation of composite rock-mortar specimens based on SHPB tests. *Int. J. Min. Sci. Technol.* **2022**, *32*, 793–806. [\[CrossRef\]](#)

25. Wu, Y.; Liu, X.; Tan, Y.; Ma, Q.; Fan, D.; Yang, M.; Wang, X.; Li, G. Mechanical Properties and Failure Mechanism of Anchored Bedding Rock Material under Impact Loading. *Materials* **2022**, *15*, 6560. [[CrossRef](#)]
26. Luo, S.; Gong, F. Evaluation of rock burst proneness considering specimen shape by storable elastic strain energy. *Deep Undergr. Sci. Eng.* **2022**, *1*, 116–130. [[CrossRef](#)]
27. Ji, H.G.; Ma, H.S.; Wang, J.A.; Zhang, Y.H.; Cao, H. Mining disturbance effect and mining arrangements analysis of near-fault mining in high tectonic stress region. *Saf. Sci.* **2012**, *50*, 649–654. [[CrossRef](#)]
28. Ma, J.; Zhao, J.; Lin, Y.; Liang, J.; Chen, J.; Chen, W.; Huang, L. Study on Tamped Spherical Detonation-Induced Dynamic Responses of Rock and PMMA Through Mini-chemical Explosion Tests and a Four-Dimensional Lattice Spring Model. *Rock Mech. Rock Eng.* **2023**, *56*, 7357–7375. [[CrossRef](#)]
29. Sainoki, A.; Schwartzkopff, A.K.; Jiang, L.; Mitri, H.S. Numerical Modeling of Complex Stress State in a Fault Damage Zone and Its Implication on Near-Fault Seismic Activity. *J. Geophys. Res. Solid Earth* **2021**, *126*, e2021JB021784. [[CrossRef](#)]
30. Skrzypkowski, K.; Zagórski, K.; Zagórska, A.; Apel, D.B.; Wang, J.; Xu, H.; Guo, L. Choice of the Arch Yielding Support for the Preparatory Roadway Located near the Fault. *Energies* **2022**, *15*, 3774. [[CrossRef](#)]
31. Wang, H.; Shi, R.; Song, J.; Tian, Z.; Deng, D.; Jiang, Y. Mechanical model for the calculation of stress distribution on fault surface during the underground coal seam mining. *Int. J. Rock Mech. Min. Sci.* **2021**, *144*, 104765. [[CrossRef](#)]
32. Ma, J.; Chen, J.; Chen, W.; Huang, L. A coupled thermal-elastic-plastic-damage model for concrete subjected to dynamic loading. *Int. J. Plast.* **2022**, *153*, 103279. [[CrossRef](#)]
33. Zhang, S.; Xu, X.; Zhao, X.; Zhou, X.; Huang, P. Study on excavation unloading; rheology and supporting time of soft rock in deep buried cavern. *J. China Three Gorges Univ. (Nat. Sci.)* **2020**, *42*, 57–62.
34. Dokht, R.M.; Smith, B.; Kao, H.; Visser, R.; Hutchinson, J. Reactivation of an intraplate fault by mine-blasting events: Implications to regional seismic hazard in Western Canada. *J. Geophys. Res. Solid Earth* **2020**, *125*, e2020JB019933. [[CrossRef](#)]
35. Li, Z.; Wang, C.; Shan, R.; Yuan, H.; Zhao, Y.; Wei, Y. Study on the influence of the fault dip angle on the stress evolution and slip risk of normal faults in mining. *Bull. Eng. Geol. Environ.* **2021**, *80*, 3537–3551. [[CrossRef](#)]
36. Chen, X.; Li, W.; Yan, X. Analysis on rock burst danger when fully-mechanized caving coal face passed fault with deep mining. *Saf. Sci.* **2012**, *50*, 645–648. [[CrossRef](#)]
37. Wu, Q.; Wu, Q.; Yuan, A.; Wu, Y. Analysis of mining effect and fault stability under the influence of normal faults. *Geotech. Geol. Eng.* **2021**, *39*, 49–63. [[CrossRef](#)]
38. Gu, S.C.; Wang, B.N.; Huang, R.B.; Miao, Y. Method for determining the load on and width of coal pillar at the recovery room end of fully-mechanized longwall mining. *J. China Univ. Min. Technol.* **2015**, *44*, 990–995.
39. Zhu, R.; Yue, X.; Liu, X.; Shi, Z.; Li, X. Study on Influencing Factors of Ground Pressure Behavior in Roadway-Concentrated Areas under Super-Thick Nappe. *Materials* **2023**, *16*, 89. [[CrossRef](#)] [[PubMed](#)]
40. Jiao, Z.; Wang, L.; Zhang, M.; Wang, J. Numerical Simulation of Mining-Induced Stress Evolution and Fault Slip Behavior in Deep Mining. *Adv. Mater. Sci. Eng.* **2021**, *2021*, 8276408. [[CrossRef](#)]
41. Yang, S.Q.; Chen, M.; Jing, H.W.; Chen, K.F.; Meng, B. A case study on large deformation failure mechanism of deep soft rock roadway in Xin'An coal mine, China. *Eng. Geol.* **2017**, *217*, 89–101. [[CrossRef](#)]
42. Yan, S.; Zhang, D.; Bai, J.; Guo, Y. Research on the Stability of Surrounding Rock and Active Passive Joint Control Technology in the Retraction Tunnel. *J. Min. Saf. Eng.* **2023**, *40*, 774–785.
43. Wang, B. Research on the Deformation and Failure Mechanism of Surrounding Rock in the Retraction Tunnel and Its Control Technology. Ph.D. Thesis, Xi'an University of Science and Technology, Xi'an, China, 2017.
44. Fan, D.; Liu, X.; Tan, Y.; Li, X.; Lkhamsuren, P. Instability energy mechanism of super-large section crossing chambers in deep coal mines. *Int. J. Min. Sci. Technol.* **2022**, *32*, 1075–1086. [[CrossRef](#)]
45. Zhang, D.; Duan, Y.; Du, W.; Chai, J. Experimental Study on Physical Similar Model of Fault Activation Law Based on Distributed Optical Fiber Monitoring. *Shock Vib.* **2021**, *2021*, 4846977. [[CrossRef](#)]
46. Wang, H.; Jiang, Y.; Xue, S.; Mao, L.; Lin, Z.; Deng, D.; Zhang, D. Influence of fault slip on mining-induced pressure and optimization of roadway support design in fault-influenced zone. *J. Rock Mech. Geotech. Eng.* **2016**, *8*, 660–671. [[CrossRef](#)]
47. Liu, X.; Wu, Y.; Tan, Y.; Yang, M.; Li, G.; Xie, C. Mechanism of inclined anchor rod fracture and timing of strengthening support in deep high-level stress tunnels. *J. Coal Ind.* **2023**, *48*, 609–622.
48. Yalong, L.; Ahmed, M.A.; Cheng, L. Support design of main retracement passage in fully mechanised coal mining face based on numerical simulation. *Appl. Math. Nonlinear Sci.* **2021**, *7*, 553–560.
49. Jin, Y.; Geng, J.; Lv, C.; Chi, Y.; Zhao, T. A methodology for equipment condition simulation and maintenance threshold optimization oriented to the influence of multiple events. *Reliab. Eng. Syst. Saf.* **2023**, *229*, 108879. [[CrossRef](#)]

Disclaimer/Publisher's Note: The statements, opinions and data contained in all publications are solely those of the individual author(s) and contributor(s) and not of MDPI and/or the editor(s). MDPI and/or the editor(s) disclaim responsibility for any injury to people or property resulting from any ideas, methods, instructions or products referred to in the content.